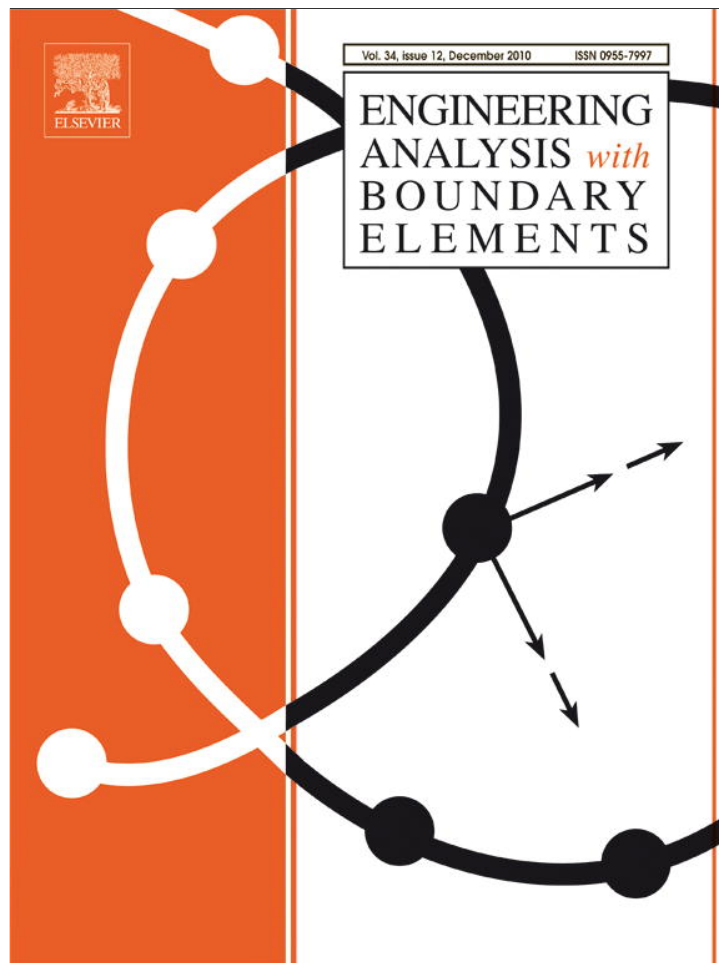


Provided for non-commercial research and education use.
Not for reproduction, distribution or commercial use.



This article appeared in a journal published by Elsevier. The attached copy is furnished to the author for internal non-commercial research and education use, including for instruction at the authors institution and sharing with colleagues.

Other uses, including reproduction and distribution, or selling or licensing copies, or posting to personal, institutional or third party websites are prohibited.

In most cases authors are permitted to post their version of the article (e.g. in Word or Tex form) to their personal website or institutional repository. Authors requiring further information regarding Elsevier's archiving and manuscript policies are encouraged to visit:

<http://www.elsevier.com/copyright>



ELSEVIER

Contents lists available at ScienceDirect

Engineering Analysis with Boundary Elements

journal homepage: www.elsevier.com/locate/enganabound

Analysis of three-dimensional natural convection of nanofluids by BEM

J. Ravnik*, L. Škerget, M. Hriberšek

Faculty of Mechanical Engineering, University of Maribor, Smetanova 17, SI-2000 Maribor, Slovenia

ARTICLE INFO

Article history:

Received 25 March 2010

Accepted 24 June 2010

Available online 31 July 2010

Keywords:

Nanofluids

Boundary element method

Fluid flow

Heat transfer

Velocity–vorticity

Dynamic solver accuracy algorithm

ABSTRACT

In this paper we analyse flow and heat transfer characteristics of nanofluids in natural convection flows in closed cavities. We consider two test cases: natural convection in a three-dimensional differentially heated cavity, and flow around a hotstrip located in two positions within a cavity. Simulations were performed for Rayleigh number values ranging from 10^3 to 10^6 . Performance of three types of water based nanofluids was compared with pure water and air. Stable suspensions of Cu, Al_2O_3 and TiO_2 solid nanoparticles in water were considered for different volume fractions ranging up to 20%. We present and compare heat flux for all cases and analyse heat transfer enhancement attributed to nanofluids in terms of their enhanced thermal properties and changed flow characteristics. Results show that, using nanofluids, the largest heat transfer enhancements can be achieved in conduction dominated flows as well as that nanofluids increase the three-dimensional character of the flow field. We additionally examine the relationship between vorticity, vorticity flux and heat transfer for flow of nanofluids.

The simulations were performed using a three-dimensional boundary element method based flow solver, which has been adapted for the simulation of nanofluids. The numerical algorithm is based on the combination of single domain and subdomain boundary element method, which are used to solve the velocity–vorticity formulation of Navier–Stokes equations. In the paper we present the adaptation of the solver for simulation of nanofluids. Additionally, we developed a dynamic solver accuracy algorithm, which was used to speed up the simulations.

© 2010 Elsevier Ltd. All rights reserved.

1. Introduction

With the advancement of engineering technology there comes an increasing demand for cooling. Efficient cooling is one of the most important challenges. Low thermal conductivity of working fluids such as water, oil or ethylene glycol led to the introduction of nanofluids, which represent a novel approach to cooling. Nanofluid is a suspension consisting of uniformly dispersed and suspended nanometre-sized (10–50 nm) particles in base fluid, pioneered by Choi [6]. Nanofluids have very high thermal conductivities at very low nanoparticle concentrations and exhibit considerable enhancement of convection [35]. Intensive research in the field of nanofluids started only a decade ago. A wide variety of experimental and theoretical investigations have been performed, as well as several nanofluid preparation techniques have been proposed [33].

Buoyancy induced flow and heat transfer is an important phenomenon used in various engineering systems. Several researchers have been focusing on buoyant flow of nanofluids. Oztop and Abu-Nada [20] performed a two-dimensional study of

natural convection of various nanofluids in partially heated rectangular cavities, reporting that the type of nanofluid is a key factor for heat transfer enhancement. They obtained best results with Cu nanoparticles. The same researchers [2] examined the effects of inclination angle on natural convection in enclosures filled with Cu–water nanofluid. They reported that the effect of nanofluid on heat enhancement is more pronounced at low Rayleigh numbers. Hwang et al. [13] studied natural convection of a water based Al_2O_3 nanofluid in a rectangular cavity heated from below. They investigated convective instability of the flow and heat transfer and reported that the natural convection of a nanofluid becomes more stable when the volume fraction of nanoparticles increases. Ho et al. [12] studied effects on nanofluid heat transfer due to uncertainties of viscosity and thermal conductivity in a buoyant enclosure. They demonstrated that usage of different models for viscosity and thermal conductivity does indeed have a significant impact on heat transfer. Natural convection of nanofluids in an inclined differentially heated square enclosure was studied by Ögüt [19], using polynomial differential quadrature method.

Forced and mixed convection studies were also performed. Abu-Nada [1] studied the application of nanofluids for heat transfer enhancement of separated flows encountered in a backward facing step. He found that the high heat transfer inside the recirculation zone depends mainly on thermophysical

* Corresponding author.

E-mail addresses: jure.ravnik@uni-mb.si (J. Ravnik), leo@uni-mb.si (L. Škerget), matjaz.hribersek@uni-mb.si (M. Hriberšek).

properties of nanoparticles and that it is independent of Reynolds number. Mirmasoumi and Behzadmehr [18] numerically studied the effect of nanoparticle mean diameter on mixed convection heat transfer of a nanofluid in a horizontal tube using a two-phase mixture model. They showed that the convective heat transfer could be significantly increased by using particles with smaller mean diameter. Akbarinia and Behzadmehr [3] numerically studied laminar mixed convection of a nanofluid in horizontal curved tubes. Tiwari and Das [30] studied heat transfer in a lid-driven differentially heated square cavity. They reported that the relationship between heat transfer and the volume fraction of solid particles in a nanofluid is nonlinear. Torii [31] experimentally studied turbulent heat transfer behaviour of nanofluid in a circular tube, heated under constant heat flux. He reported that the relative viscosity of nanofluids increases with concentration of nanoparticles, pressure loss of nanofluids is slightly larger than that of pure fluid and that heat transfer enhancement is affected by occurrence of particle aggregation.

Numerous numerical methods have been proposed to simulate the natural convection phenomena. Stream function-vorticity formulation was used for simulation of nanofluids in two dimensions by Gümgüm and Tezer-Sezgin [11]. In this work we employ the velocity–vorticity formulation of Navier–Stokes equations, written for nanofluids coupled with the energy equation. The unknown field functions are the velocity, vorticity and temperature. We employ the boundary element method (BEM) to find the solution. Daube [9] stated that accurate determination of boundary values of vorticity is essential for conservation of mass when using the velocity–vorticity form of the governing equations. Several different approaches have been proposed for the determination of vorticity on the boundary. Wong and Baker [34] used a second-order Taylor series to determine the boundary vorticity values explicitly. Daube [9] used an influence matrix technique to enforce both, the continuity equation and the definition of the vorticity in the treatment of the two-dimensional incompressible Navier–Stokes equations. Liu [15] recognised that the problem is even more severe when he extended it to three dimensions. Lo et al. [16] used the differential quadrature method. We use single domain BEM to solve the kinematics equation for boundary vorticity values [29]. Apart from the boundary vorticity values, all other flow fields are solved by subdomain BEM [22,23]. Subdomain BEM solution of a partial differential equation leads to an overdetermined sparse system of linear equations. A sparse system enables fast algebraic operations and does not require a lot of storage.

2. Governing equations

We consider water based nanofluids. Their thermophysical properties are given in Table 1. Water and nanoparticles are in thermal equilibrium and no slip occurs between them. We assume the nanofluid to be incompressible. Natural convection exhibited by the nanofluids in our simulations is laminar. Effective properties of the nanofluid are: density ρ_{nf} , dynamic

viscosity μ_{nf} , heat capacitance $(c_p)_{nf}$, thermal expansion coefficient β_{nf} and thermal conductivity k_{nf} , where subscript nf is used to denote effective, i.e. nanofluid properties. The properties are all assumed constant throughout the flow domain. The mass conservation law for an incompressible fluid may be stated as

$$\vec{\nabla} \cdot \vec{v} = 0. \quad (1)$$

Considering constant nanofluid material properties and taking density variation into account within the Boussinesq approximation we write the momentum equation as

$$\frac{\partial \vec{v}}{\partial t} + (\vec{v} \cdot \vec{\nabla})\vec{v} = -\beta_{nf}(T-T_0)\vec{g} - \frac{1}{\rho_{nf}}\vec{\nabla}p + \frac{\mu_{nf}}{\rho_{nf}}\nabla^2\vec{v}. \quad (2)$$

We assume that no internal energy sources are present in the fluid. We will not deal with high velocity flow of highly viscous fluid, hence we will neglect irreversible viscous dissipation. With this, the internal energy conservation law, written with temperature as the unknown variable, reads as

$$\frac{\partial T}{\partial t} + (\vec{v} \cdot \vec{\nabla})T = \frac{k_{nf}}{(\rho c_p)_{nf}}\nabla^2 T. \quad (3)$$

Relationships between properties of nanofluid to those of pure fluid and pure solid are provided with the following models. Density of the nanofluid is calculated using particle volume fraction ϕ and densities of pure fluid ρ_f and of solid nanoparticles ρ_s as

$$\rho_{nf} = (1-\phi)\rho_f + \phi\rho_s. \quad (4)$$

The effective dynamic viscosity of a fluid of dynamic viscosity μ_f containing a dilute suspension of small rigid spherical particles, is given by Brinkman [4] as

$$\mu_{nf} = \frac{\mu_f}{(1-\phi)^{2.5}}. \quad (5)$$

Several other models exist (such as the Einstein model [10]), which are based on experimental measurements or theoretical investigations.

The heat capacitance of the nanofluid can be expressed as [14]

$$(\rho c_p)_{nf} = (1-\phi)(\rho c_p)_f + \phi(\rho c_p)_s. \quad (6)$$

Similarly, the nanofluid thermal expansion coefficient can be written as $(\rho\beta)_{nf} = (1-\phi)(\rho\beta)_f + \phi(\rho\beta)_s$, which may be, by taking into account the definition of ρ_{nf} , written as

$$\beta_{nf} = \beta_f \left[\frac{1}{1 + \frac{\phi\rho_s}{\rho_f}} \frac{\beta_s}{(1-\phi)\rho_f} + \frac{1}{1 + \frac{\phi\rho_s}{\rho_f}} \right]. \quad (7)$$

The effective thermal conductivity of the nanofluid is approximated by the Maxwell–Garnett formula [17]

$$k_{nf} = k_f \frac{k_s + 2k_f - 2\phi(k_f - k_s)}{k_s + 2k_f + \phi(k_f - k_s)}. \quad (8)$$

This formula is valid only for spherical particles, since it does not take into account the shape of particles. Thus, our macroscopic modelling of nanofluids is restricted to spherical nanoparticles and it is suitable for small temperature gradients [28].

2.1. Nondimensional equations in velocity–vorticity form

Vorticity, $\vec{\omega}$, is defined as a curl of velocity. By taking the curl of the mass conservation law (1) and of the momentum transport equation (2) and taking into account that by definition vorticity is solenoidal, $\vec{\nabla} \cdot \vec{\omega} = 0$, we derive the velocity–vorticity formulation of Navier–Stokes equations. The equations are rewritten into

Table 1
Thermophysical properties of water based nanofluids [20].

	Pure water	Cu	Al ₂ O ₃	TiO ₂
c_p (J/kg K)	4179	385	765	686.2
ρ (kg/m ³)	997.1	8933	3970	4250
k (W/m K)	0.613	400	40	8.9538
β ($\times 10^{-5}$ K ⁻¹)	21	1.67	0.85	0.9
α ($\times 10^{-7}$ m ² /s)	1.47	1163	131.7	30.7

nondimensional form using

$$\begin{aligned} \vec{v} &\rightarrow \frac{\vec{v}}{v_0}, \quad \vec{r} \rightarrow \frac{\vec{r}}{L}, \quad \omega \rightarrow \frac{\omega L}{v_0}, \quad t \rightarrow \frac{v_0 t}{L}, \quad T \rightarrow \frac{T-T_0}{\Delta T}, \quad \vec{g} \rightarrow \frac{\vec{g}}{g_0}, \\ v_0 &= \frac{k_f}{(\rho c_p)_f L}, \end{aligned} \quad (9)$$

where T_0 and L are characteristic velocity and temperature. Characteristic temperature difference is ΔT , while $g_0=9.81 \text{ m/s}^2$. We define pure fluid Rayleigh and Prandtl number values as

$$Ra = \frac{g_0 \beta_f \Delta T L^3 \rho_f (\rho c_p)_f}{\mu_f k_f}, \quad Pr = \frac{\mu_f c_p}{k_f}. \quad (10)$$

The choice for characteristic velocity v_0 in (9) is common for buoyant flow simulations. It ensures that the Reynolds number is eliminated for the governing equations, since its value multiplied by Prandtl number equals one. With this the nondimensional velocity–vorticity formulation of Navier–Stokes equations for simulation of nanofluids consists of the kinematics equation, the vorticity transport equation and the energy equation:

$$\nabla^2 \vec{v} + \vec{\nabla} \times \vec{\omega} = 0, \quad (11)$$

$$\frac{\partial \vec{\omega}}{\partial t} + (\vec{v} \cdot \vec{\nabla}) \vec{\omega} = (\vec{\omega} \cdot \vec{\nabla}) \vec{v} + Pr \frac{\mu_{nf}}{\mu_f} \frac{\rho_f}{\rho_{nf}} \nabla^2 \vec{\omega} - Pr Ra \frac{\beta_{nf}}{\beta_f} \vec{\nabla} \times T \vec{g}, \quad (12)$$

$$\frac{\partial T}{\partial t} + (\vec{v} \cdot \vec{\nabla}) T = \frac{k_{nf}}{k_f} \frac{(\rho c_p)_f}{(\rho c_p)_{nf}} \nabla^2 T. \quad (13)$$

The flow and heat transfer of a nanofluid is thus defined by specifying the pure fluid Rayleigh and Prandtl number values. The nanofluid properties are evaluated using the following models: ρ_{nf}/ρ_f from (4), μ_{nf}/μ_f from (5), $(\rho c_p)_{nf}/(\rho c_p)_f$ from (6), β_{nf}/β_f from (7) and k_{nf}/k_f from (8). We should note that the effective viscosity is independent of nanoparticle type, attributing expected differences in results to heat related physical parameters only.

3. Numerical method

The algorithm used to solve the set of governing equations (11)–(13) is devised as follows. Either Dirichlet or Neumann type boundary conditions for velocity and temperature must be known. In this paper we use the no-slip boundary condition on all solid walls and prescribe temperature or temperature flux. Boundary conditions for vorticity are unknown and are calculated as a part of the algorithm. The following steps are performed.

1. Use models (4)–(8) to calculate ratios of nanofluid to pure fluid material properties.
2. Calculate vorticity values on the boundary by single domain BEM from the kinematics Eq. (11).
3. Calculate velocity values by sub-domain BEM from the kinematics equation (11).
4. Calculate temperature values by sub-domain BEM from the energy equation (13).
5. Calculate vorticity values in the domain by sub-domain BEM from the vorticity transport equation (12).
6. Check convergence. If all flow fields converged to 10^{-6} stop, else go to 2.

The three-dimensional solver capable of simulating flow and heat transfer by solving velocity–vorticity formulation of Navier–Stokes equations by a combination of single and sub-domain BEM was

developed by Ravnik et al. [26,25]. The single domain BEM has been accelerated by the use of the Fast multipole method [27].

The solver has been adapted for simulation of flow and heat transfer of nanofluids. Governing equations are written in integral form. The integral form of equations is obtained by using Green's second identity for the unknown field function and for the fundamental solution u^* of the diffusion operator: $u^* = 1/4\pi|\vec{\xi}-\vec{r}|$. Green's second identity is an integral equation that can be, through a limiting process, rewritten in a form that enables calculation of a field function in a source point $\vec{\xi}$.

The integral form of the kinematics equation is

$$\begin{aligned} c(\vec{\xi}) \vec{n}(\vec{\xi}) \times \vec{v}(\vec{\xi}) + \vec{n}(\vec{\xi}) \times \int_{\Gamma} \vec{v} \vec{\nabla} u^* \cdot \vec{n} d\Gamma \\ = \vec{n}(\vec{\xi}) \times \int_{\Gamma} \vec{v} \times (\vec{n} \times \vec{\nabla}) u^* d\Gamma + \vec{n}(\vec{\xi}) \times \int_{\Omega} (\vec{\omega} \times \vec{\nabla} u^*) d\Omega, \end{aligned} \quad (14)$$

where $\vec{\xi}$ is the source or collocation point, \vec{n} is a vector normal to the boundary, pointing out of the domain. $c(\vec{\xi})$ is the geometric factor defined as $c(\vec{\xi}) = \alpha/4\pi$, where α is the inner angle with origin in $\vec{\xi}$. In order to write a linear system of equations for the unknown boundary vorticity values, we set the source point into every boundary node of the whole computational domain. This yields a full system matrix where number of rows and columns is equal to number of boundary nodes. This, tangential form of the kinematics equation is used to determine boundary vorticity values. After discretization the system matrix is formed in such a way that boundary values of vorticity are unknown, while domain vorticity and velocity values are taken from the previous nonlinear iteration. The system is solved using a LU decomposition method.

In the algorithm the kinematics equation is used again to determine domain velocity values. The following form is used:

$$c(\vec{\xi}) \vec{v}(\vec{\xi}) + \int_{\Gamma} \vec{v} \vec{\nabla} u^* \cdot \vec{n} d\Gamma = \int_{\Gamma} \vec{v} \times (\vec{n} \times \vec{\nabla}) u^* d\Gamma + \int_{\Omega} (\vec{\omega} \times \vec{\nabla} u^*) d\Omega. \quad (15)$$

Solution is obtained by sub-domain BEM. Boundary values of velocity are known boundary conditions, while domain and boundary values of vorticity are assumed known from the previous iteration.

The partial derivative with respect to time in the kinetics equations is approximated by second order three point finite difference scheme $\partial T/\partial t = (3T-4T'+T'')/2\Delta t$, where Δt is the time step and prime and double prime denote field functions in two earlier time steps. Choice of the time step depends on the problem being solved. It should be small enough to capture the physical behaviour of the flow, i.e. be smaller than the characteristic length scale of the flow divided by the characteristic velocity. In case of simulation of steady phenomena a single very large time step is chosen ($\Delta t = 10^{16}$). The final forms of vorticity transport and energy equation are

$$\begin{aligned} c(\vec{\xi}) \omega_j(\vec{\xi}) + \int_{\Gamma} \omega_j \vec{\nabla} u^* \cdot \vec{n} d\Gamma \\ = \int_{\Gamma} u^* q_j d\Gamma + \frac{1}{Pr} \frac{\mu_f \rho_{nf}}{\mu_{nf} \rho_f} \left(\int_{\Gamma} \vec{n} \cdot \{u^* (\vec{v} \omega_j - \vec{\omega} v_j)\} d\Gamma \right. \\ \left. - \int_{\Omega} (\vec{v} \omega_j - \vec{\omega} v_j) \cdot \vec{\nabla} u^* d\Omega \right) - Ra \frac{\beta_{nf} \mu_f \rho_{nf}}{\beta_f \mu_{nf} \rho_f} \int_{\Gamma} (u^* T \vec{g} \times \vec{n})_j d\Gamma \\ - Ra \frac{\beta_{nf} \mu_f \rho_{nf}}{\beta_f \mu_{nf} \rho_f} \int_{\Omega} (T \vec{\nabla} \times u^* \vec{g})_j d\Omega \\ + \frac{1}{Pr} \frac{\mu_f \rho_{nf}}{\mu_{nf} \rho_f} \frac{1}{2\Delta t} \int_{\Omega} (3\omega_j - 4\omega'_j + \omega''_j) u^* d\Omega, \\ c(\vec{\xi}) T(\vec{\xi}) + \int_{\Gamma} T \vec{\nabla} u^* \cdot \vec{n} d\Gamma \end{aligned} \quad (16)$$

$$\begin{aligned}
 &= \int_{\Gamma} u^* T_q d\Gamma + \frac{k_f (\rho c_p)_{nf}}{k_{nf} (\rho c_p)_f} \left(\int_{\Gamma} \vec{n} \cdot \{u^*(\vec{\nabla}T)\} d\Gamma - \int_{\Omega} (\vec{\nabla}T) \cdot \vec{\nabla}u^* d\Omega \right) \\
 &+ \frac{k_f (\rho c_p)_{nf}}{k_{nf} (\rho c_p)_f} \frac{1}{2\Delta t} \int_{\Omega} (3T - 4T' + T'') u^* d\Omega. \quad (17)
 \end{aligned}$$

In the subdomain BEM method we make a mesh of the entire domain Ω and name each mesh element a subdomain. Eqs. (15)–(17) are written for each of the subdomains. In order to obtain a discrete version of the equations, we use shape functions to interpolate field functions and flux across the boundary and inside of the subdomain. In this work we used hexahedral subdomains with 27 nodes, which enable continuous quadratic interpolation of field functions. The boundary of each hexahedron consists of six boundary elements. On each boundary element we interpolate the flux using discontinuous linear interpolation scheme with four nodes. By using discontinuous interpolation we avoid flux definition problems in corners and edges. A function, e.g. temperature, is interpolated over a boundary element as $T = \sum \phi_i T_i$, inside each subdomain as $T = \sum \Phi_i T_i$, while flux is interpolated over boundary elements as $q = \sum \phi_i q_i$.

3.1. Acceleration of computation

The numerical algorithm solves the above equations sequentially within a time step. At the end of each iteration, RMS difference between flow fields of current and previous iteration is calculated. We define the RMS difference as the sum of squared difference between flow field values of current and previous iteration for each node divided by the sum of squares of nodal values in the previous iteration. When RMS difference for all flow fields reaches $\varepsilon_{err} = 10^{-6}$, we stop to iterate. Within each iteration 10 systems of linear equations must be solved (three for boundary vorticity values, three for domain velocity, three for domain vorticity and one for temperature). Apart from the flow kinematics, each system of linear equations is solved by the LSQR solver [21] with diagonal preconditioning. The solver requires a large number of iterations in order to converge to a predefined convergence criteria ε . The original algorithm, as proposed by Ravnik et al. [26], uses a constant convergence criteria. Value, which is 10 times less than the required RMS criteria ε_{err} was usually used, i.e. $\varepsilon = \varepsilon_{err}/10 = 10^{-7}$.

We argue that it is not necessary to keep $\varepsilon = 10^{-7}$ during the whole iterative process, since at the beginning, when RMS differences ε_{err} are large, we do not require a very accurate solution of linear systems of equations. Considering this ε may be set larger. Since the number of iterations of the solver of linear systems of equation depends strongly on the required accuracy and since the most CPU time is used in these routines, we anticipate a large decrease of CPU time.

In order to accelerate the solver, we used the following steps. Instead of keeping ε constant, we change its value every iteration. We set the range for ε between $\varepsilon_{min} = 10^{-7}$ and $\varepsilon_{max} = 10^{-3}$. The maximal value was chosen so that we ensure that at least some work is done by the solver in each iteration. We introduce a parameter R ; $1 \leq R \leq 100$. At the end of each iteration, we calculate RMS differences ε_{err} for all flow fields and use the following algorithm to determine the new ε :

DO \forall equations

$\varepsilon_{old} = \varepsilon$

IF $(\varepsilon_{err}/R < \varepsilon)$ THEN $\varepsilon = \varepsilon_{err}/R$ ELSE $\varepsilon = \varepsilon_{max}$

IF $(\varepsilon_{old} < \varepsilon)$ $\varepsilon = \varepsilon_{old}$

IF $(\varepsilon < \varepsilon_{min})$ $\varepsilon = \varepsilon_{min}$

END DO

We keep the linear solver accuracy between the minimum and maximum value at $\varepsilon = \varepsilon_{err}/R$. In the algorithm we do not allow for decrease of linear solver accuracy. If at some stage during the nonlinear loop RMS difference increases, the linear solver accuracy is not increased. This rule was included in the algorithm because we want to limit such behaviour as much as possible, thus it seems prudent to not allow for linear solver accuracy decrease.

4. Test cases

We used the developed numerical algorithm to simulate natural convection of nanofluids in two configurations: firstly, a cubic cavity is filled with fluid and subjected to a temperature difference on two opposite vertical sides. Secondly, the source of natural convection is a hotstrip located in a cubic cavity. Its height is one half of the cavity's height. Two sides of the cavity are cooled, the other four are adiabatic. Sketches and boundary conditions for both cases are shown in Fig. 1. Both cases were investigated for air ($Pr=0.71$), water ($Pr=6.2$) and water based nanofluids (Table 1) for several Rayleigh number values. The hotstrip was positioned in the centre of the cavity ($d=0.4H$) and off-centre ($d=0.5H$).

Natural convection of air and other pure fluids in a differentially heated cavity has been under intense investigation in the past. More recently several authors simulated nanofluids in this case [2,13,12,30]. Simulation conditions varied—in some cases the hot side of the cavity was smaller, in others the cavity was inclined. All of this work with nanofluids was done in two-dimensional. In this paper we present three-dimensional results. In our previous work [25] we examined this problem using air as the working fluid. We established, by comparison with other authors [32], that a grid with 25^3 nodes was sufficient. In this paper we increased the grid density to 41^3 nodes in order to further increase the accuracy of computations. Nodes were concentrated towards the hot and cold walls in such a way that the ratio between the largest and the smallest element length was 7.

Corvaro and Paroncini [8,7] performed a two-dimensional PIV experiment on a hotstrip problem, using air as the working fluid. The width and height of their enclosure were $H=0.05$ m. The depth of the enclosure was 0.42 m, with which they achieved a two-dimensional flow field. They measured the flow field in the central plane of the enclosure for Rayleigh number values between $Ra=6.39 \times 10^4$ and 3.16×10^5 . Preliminary results of

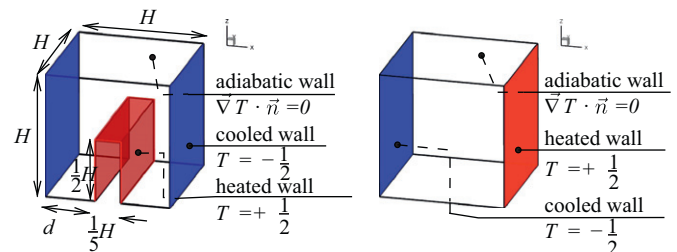


Fig. 1. Setup and boundary conditions of the hotstrip problem (left) and differentially heated cavity problem (right). Hotstrip of height $0.5H$ and width $0.2H$ is located at distance d from the left cold wall. The hotstrip is heated to $T = +0.5$, while the walls at $x=0$ and H are cooled to $T = -0.5$. There is no temperature flux through all other walls. In differentially heated cavity we keep two opposite vertical walls cold and hot, while all other walls are adiabatic. No-slip velocity boundary conditions are applied on all walls.

numerical simulations of air in the hotstrip test case were presented by Ravnik and Škerget [24]. A grid of $51 \times 31 \times 13$ nodes proved successful for air simulations. For nanofluids simulations in this work, we selected a denser mesh having $61 \times 49 \times 19$ nodes.

5. Results

The heat transfer of a nanofluid is expected to depend, apart from the flow configuration, on a number of material factors, such as thermal conductivity and heat capacitance of both pure fluid and particles, volume fraction, viscosity, etc. In order to compare effectiveness of nanofluids in different simulations, wall heat flux is calculated. Usually, the heat flux \dot{Q} is expressed in terms of pure fluid thermal conductivity, characteristic flow scales and a nondimensional Nusselt number, i.e. $\dot{Q} = k_f \Delta T \cdot Nu$. The Nusselt number, Nu , is defined as the integral of the temperature flux through a wall. For a nanofluid, it is written as

$$Nu = \frac{k_{nf}}{k_f} \int_{\Gamma} \vec{\nabla} T \cdot \vec{n} d\Gamma, \tag{18}$$

where Γ is the surface through which we calculate the heat flux and \vec{n} is a unit normal to this surface. We study local variation of heat flux using the local Nusselt number defined as $Nu_l(x,y,z) = k_{nf} / k_f \vec{\nabla} T \cdot \vec{n}$.

5.1. Testing of dynamic solver accuracy algorithm

The algorithm has been tested on the hotstrip example. Air was the working fluid. Simulations were run for $Ra=10^3, 10^4$ and 10^5 using parameter R ranging between $R=0.1$ and 100. Table 2 shows the number of iterations of the LSQR solver [21], CPU time and the number of iterations of the nonlinear loop. Within each nonlinear loop iteration, seven linear systems of equations must be solved using LSQR solver. The table presents cumulative values for number of LSQR iterations.

At $Ra=10^3$, the total number of iterations of the LSQR solver required for the computation to converge, which is equal to 103 thousand when solver accuracy is constant at $\epsilon = 10^{-7}$, drops to more than one half of this value when using newly proposed dynamic solver accuracy algorithm with $R=1$. At the same time, the CPU time of the whole nonlinear loop was decreased from 75 to 35.5 min. At $Ra=10^5$ the number of iterations was decreased

Table 2
Comparison of convergence performance and the number of iterations of LSQR solver [21] for different values of parameter R .

ϵ_{min}	ϵ_{max}	R	LSQR nit ($\times 10^3$)	CPU time (min)	No. nonlin. iterations
$Ra=10^3$					
10^{-7}	10^{-7}	–	103.5	75	131
10^{-7}	10^{-3}	100	73.6	55	132
10^{-7}	10^{-3}	10	57.2	45.7	138
10^{-7}	10^{-3}	1	37.9	35.5	154
$Ra=10^4$					
10^{-7}	10^{-7}	–	148.8	108	205
10^{-7}	10^{-3}	10	79.9	66.3	207
$Ra=10^5$					
10^{-7}	10^{-7}	–	759.9	570	1235
10^{-7}	10^{-3}	10	410.6	363	1255
10^{-7}	10^{-3}	1	202.9	228	1179
10^{-7}	10^{-3}	0.1	150.6	241	1774

All simulations were run until RMS difference reached $\epsilon_{err} = 10^{-6}$.

from 759 thousand to 202 thousand and the CPU time from 570 to 228 min. Very low values of R tend to increase the number of nonlinear iterations required to reach the solution. This causes additional CPU time to be spent in forming the right hand sides of linear systems of equations. The gain in CPU time seems to be unaffected by the nonlinearity of the problem, i.e. the Rayleigh number.

Fig. 2 shows graphs of RMS difference ϵ_{err} , number of LSQR iterations and solver accuracy ϵ versus nonlinear iteration number through the whole simulation. Comparison of simulation with and without the use of dynamic solver accuracy is presented. We observe that the convergence (the ϵ_{err} graph) is nearly identical for both cases. This proves that the use of dynamic solver accuracy algorithm does not change the convergence properties of the whole nonlinear algorithm. On the other hand, a large improvement in terms of decreasing of LSQR number of iterations can be observed when dynamic solver accuracy is used. The dynamic solver accuracy algorithm keeps the number of LSQR iterations at an approximately constant level. Without the use of dynamic solver accuracy algorithm the number of LSQR iteration is very large at the beginning of each time step and only gradually decreases. This difference is reflected on the total number of LSQR iterations and in consequence on total CPU time needed for the simulation.

Based on this analysis we decided to use dynamic solver accuracy algorithm and we chose the value $R=10$ for all further analyses.

5.2. Differentially heated cubic cavity

Applying a temperature difference on two opposite walls of an otherwise insulated cavity starts up natural convection producing a large vortex in the main part of the enclosure. At low Rayleigh number values the vortex is weak and the heat is transferred predominately with conduction. Convection dominates at $Ra=10^6$ where temperature stratification may be observed. The flow becomes unsteady for higher Ra values with vortices forming along the hot and cold walls. Due to high thermal conductivity of nanofluids we expect to observe the largest improvement in heat transfer of nanofluids for cases where conduction plays a nonnegligible role. Simulations were performed for Rayleigh number values between $Ra=10^3$ and 10^6 for pure air, pure water and three nanofluids. Two solid nanoparticle volume fractions in nanofluids were considered: $\phi = 0.1$ and 0.2.

Nusselt number values for the natural convection in a cube are shown in Table 3. The validity of our numerical method is confirmed by comparing heat flux of present results for simulation of air with the results of Lo et al. [16]. We observe about 0.1% difference in Nusselt number values.

Using water based nanofluids instead of pure water increases heat transfer in all cases. For low Rayleigh number, where conduction is the predominant heat transfer mechanism, the enhancement is the largest. For Cu nanofluid at $Ra=10^3$ we observe an 27.2% increase in heat transfer for $\phi = 0.1$ and 64.1% for $\phi = 0.2$. Similar findings were reported by Abu-Nada and Oztop [2] for two-dimensional inclined cavity case. TiO₂ nanofluid exhibits lower heat transfer enhancement, since its thermal conductivity is lower than that of Cu and Al₂O₃ nanofluids. In spite of the fact that thermal conductivity and thermal diffusivity of Al₂O₃ are about one tenth of their values for Cu, both nanofluids exhibit approximately the same heat transfer enhancement. This is due to the fact that the effective thermal diffusivity $k_{nf} / k_f \cdot (\rho c_p)_f / (\rho c_p)_{nf}$, which is the only parameter in the non-

dimensional heat equation (13), has an almost identical value for Al_2O_3 and Cu nanofluids.

As the Rayleigh number increases, convection becomes the dominant heat transfer mechanism, while conduction is negligible. Thus, the increased thermal conductivity of nanofluids plays a less important role in the overall heat balance. All nanofluids exhibit smaller heat transfer enhancement as compared to the low Rayleigh number case. At $Ra=10^6$ Cu nanofluid increases heat transfer at $\varphi = 0.1$ for 11.6% and at $\varphi = 0.2$ for 21.6%.

Fig. 3 shows the relationship between solid particle volume fraction and heat transfer. We observe for all three nanofluids that increasing solid particle volume fraction from 0.1 to 0.2 increases heat transfer. About the same increase is obtained if we compare pure

water and $\varphi = 0.1$ nanofluid. The increase in heat transfer is highest when using Cu nanofluid and lowest when using TiO_2 nanofluid.

In our geometry the hot and cold walls face each other in x direction. Thus, the main vortex, which is induced by the onset of natural convection is located in the y plane. We chose the $y=0.5H$ plane to study the two velocity profiles: vertical velocity $v_z(x,0.5H,0.5H)$ and horizontal velocity $v_x(0.5H,0.5H,z)$ across the centre of the enclosure. The comparison of profiles for $Ra=10^3$ and 10^6 for water and nanofluids is shown in Fig. 4. When conduction dominates ($Ra=10^3$) we observe that pure water reaches the highest velocities, while addition of solid particles slows down the flow. The decreased velocity results in decreased convective heat transfer. However, since in this regime the

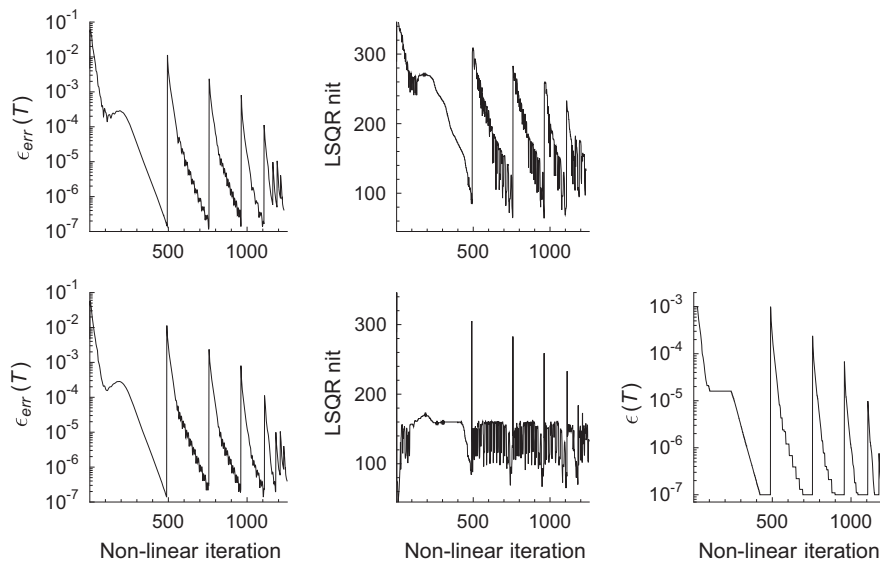


Fig. 2. The graphs show the RMS difference between flow fields of current and previous iteration, $\epsilon_{err} = 10^{-6}$, the prescribed accuracy of the LSQR solver ϵ and number of iterations of the LSQR solver. Hotstrip problem was simulated at $Ra = 10^3$; graphs show data for the temperature equation. Top row shows results of the simulation without dynamic solver accuracy ($\epsilon = 10^{-7}$); bottom row—dynamic solver accuracy algorithm was used with $R = 10$.

Table 3
Nusselt number values for the natural convection in a cube.

Ra	Air		Water	Water+Cu		Water+ Al_2O_3		Water+ TiO_2	
	[16]	Present		$\varphi = 0.1$	$\varphi = 0.2$	$\varphi = 0.1$	$\varphi = 0.2$	$\varphi = 0.1$	$\varphi = 0.2$
10^3	1.0710	1.0712	1.071	1.363	1.758	1.345	1.718	1.297	1.598
10^4	2.0537	2.0564	2.078	2.237	2.381	2.168	2.244	2.115	2.132
10^5	4.3329	4.3432	4.510	4.946	5.278	4.806	4.968	4.684	4.732
10^6	8.6678	8.6792	9.032	10.08	10.98	9.817	10.39	9.556	9.871

Solid particle volume fraction is denoted by φ . Simulations of air are compared with results of Lo et al. [16].

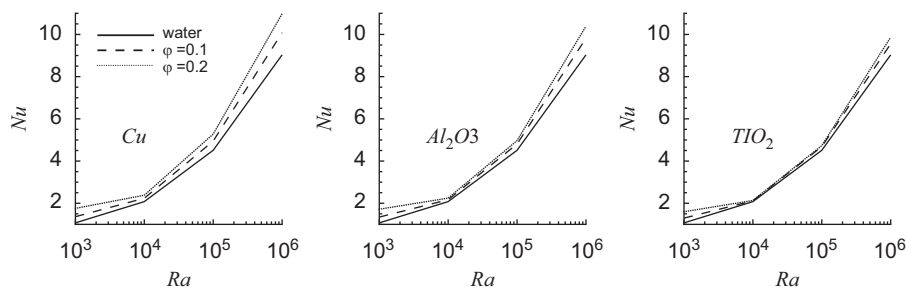


Fig. 3. Nusselt number values for natural convection in a cube. Comparing heat transfer using water and nanofluids we observe the influence of solid particle volume fraction.

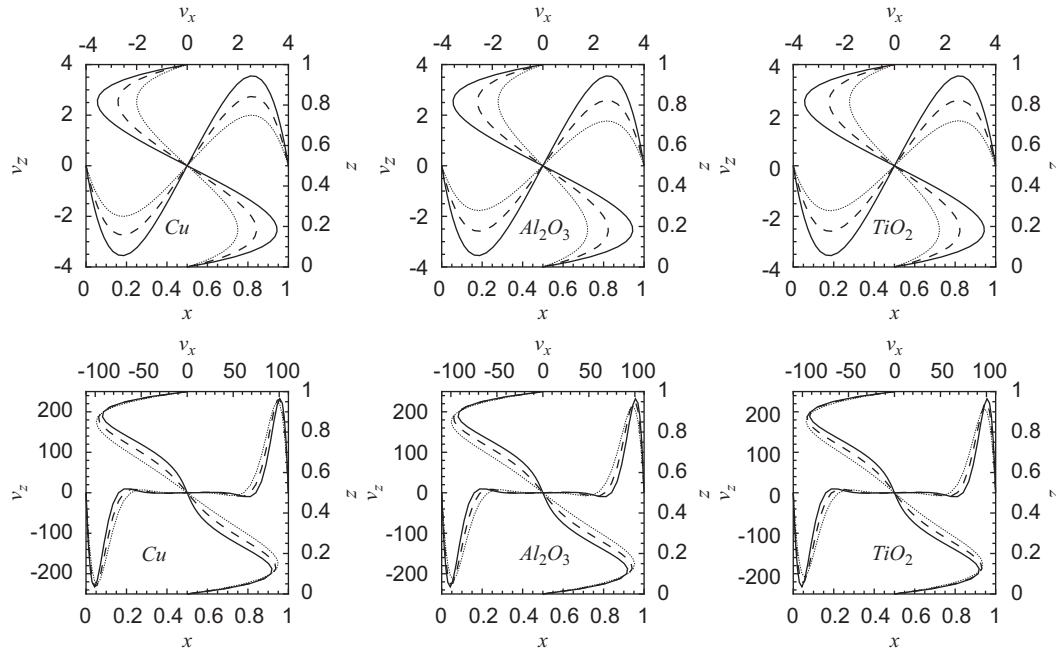


Fig. 4. Velocity profiles $v_x(z)$ and $v_z(x)$ through a centre of the $y=0.5H$ plane for natural convection in a differentially heated cubic cavity. Top row $Ra=10^3$, bottom row $Ra=10^6$. Solid line denotes pure water, dashed line $\phi=0.1$ nanofluid and dotted line $\phi=0.2$ nanofluid.

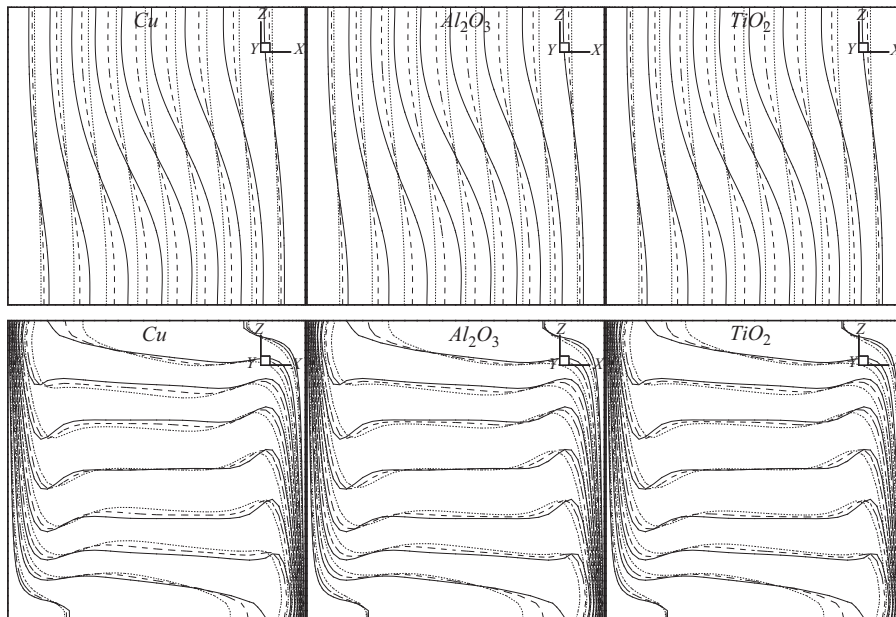


Fig. 5. Temperature contours on the central $y=0.5H$ plane for natural convection in a differentially heated cubic cavity. Contour values are $-0.4(0.1)0.4$. Top row $Ra=10^3$, bottom row $Ra=10^6$. Solid line denotes pure water, dashed line $\phi=0.1$ nanofluid and dotted line $\phi=0.2$ nanofluid.

majority of heat is transported by conduction, the decrease due to lower velocity is almost negligible and the overall heat transfer of nanofluids is still very large due to higher thermal conductivity of a nanofluid. In the $Ra=10^6$ case convection dominates. Here we observe that velocities reached by nanofluids are higher than the velocities of pure water. Thus, using nanofluids, the velocity profiles, and in consequence, temperature profiles and heat transfer are increased. The relative increase of heat transfer in the convection dominated case is smaller than the increase in the conduction dominated case because the increased thermal conductivity does not play an important role in the convection dominated heat transfer. When comparing velocity profiles

between different nanofluids we observe only slight differences. The Cu nanofluid reaches the highest velocities, while the highest velocities for Al_2O_3 nanofluid are about 4% lower and for TiO_2 approximately 9% lower.

Fig. 5 displays temperature contours in the central $y=0.5H$ plane. Comparing the temperature fields for different nanofluids we observe almost identical temperature distribution in the central part of the enclosure. Differences are larger closer to the walls, although their magnitude is still small. Since heat transfer depends on the temperature gradient on the walls, we examined the temperature contour closest to the hot and cold walls. Differences between pure fluid and nanofluid with $\phi=0.1$ or

0.2 can be observed in the conduction dominated low Rayleigh number case. We see that the low flow velocity of the high solid particle volume fraction indeed moved the first temperature contour away from the wall and thus decreased the temperature gradient. This decrease in heat transfer is much smaller than the increase obtained by the increased thermal conductivity of the nanofluid. In the convection dominated high Rayleigh number case this effect is much smaller and it does not cause a noticeable effect on the overall heat transfer.

Comparing the temperature field between different types of nanofluids we observe only minor differences. Main characteristics remain the same, i.e. approximately linear distribution of temperature contours in the conduction dominated case and stratification of temperature in the convection dominated case.

Heat flux distribution on a profile across the hot wall is shown in Fig. 6. The heat flux is smaller at the top of the hot wall and larger at the bottom, since the hot fluid is rising and decreasing the temperature gradient at the top. Comparing the $Ra=10^3$ and 10^6 cases, we see that the heat transfer enhancement is, relatively speaking, larger in the conduction dominated $Ra=10^3$ case than in the convection dominated $Ra=10^6$ case.

We examined the three-dimensional nature of the flow field. Since, in this case, the flow field is driven by a temperature difference between the two opposite walls, it causes a large predominantly two-dimensional vortex between the hot and cold walls. Three-dimensional nature of the flow can be seen in the corners of the domain. The three-dimensional nature becomes more apparent at higher Rayleigh number values. In Fig. 7 we plotted isosurfaces of absolute value of horizontal velocity component, which is perpendicular to the plane of the main vortex, i.e. $|v_y|$ in our geometry. Water and Cu nanofluid at $\phi = 0.1$ and 0.2 are compared. We observe that the v_y velocity component

grows with increasing solid particle volume fraction. Thus, usage of nanofluid tends to make the flow field more three-dimensional and contributes to the break up of symmetry and the onset of unsteadiness, which occurs at higher Rayleigh number values.

5.3. Hotstrip

The hotstrip heats the surrounding fluid inducing two main vortices—one on each side of the hotstrip. Hot fluid from the sides of the hotstrip is transported upwards by convection making the thermal boundary layer thin and thus resulting in high heat transfer. Upon reaching the top of the hotstrip the fluid flows over the top ultimately colliding with the fluid from the other side and rising upwards. When the hotstrip is located in the centre of the cavity, the flow field is symmetric and the fluid rises from the centre of the hotstrip. If the hotstrip is placed off-centre, the flow symmetry is lost. The sizes of large vortices on each side of the hotstrip are different. The flow does not rise above the centre of the hotstrip. Mixing of the fluid from both sides of the hotstrip occurs, which does not happen in the symmetric case.

Nusselt number values for the natural convection of pure fluids in a hotstrip are presented in Table 4. Tables 5 and 6 present Nusselt number values for nanofluids of two different particle volume fractions for hotstrip located in the centre ($d=0.4H$) and off-centre ($d=0.5H$). When the hotstrip is located in the centre, the flow field is symmetrical and the heat flux from both vertical walls of the hotstrip is equal. Thus in the tables we present only two values—heat flux from a vertical wall and from the top wall. In the case, when the hotstrip is located off-centre, the symmetry is broken and heat flux from all three walls is presented. Comparing heat transfer for pure fluid, air and water, we observe only minor differences. The heat transfer is only mildly improved when using water instead of air. With the addition of solid nanoparticles into the water the improvement in heat transfer is more substantial. Graph in Fig. 8 shows the total heat

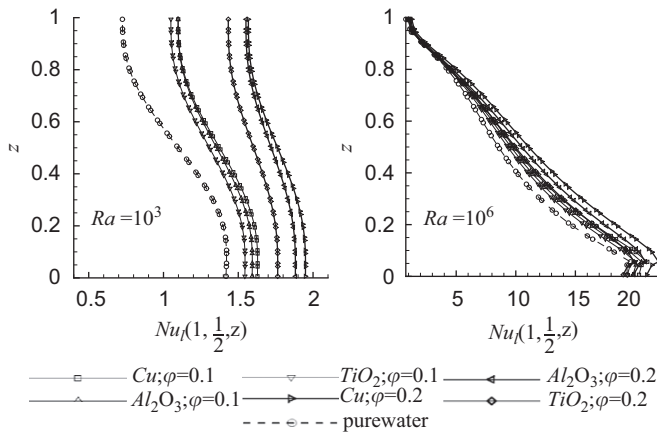


Fig. 6. Heat flux shown in terms of local Nusselt number on a profile across hot wall on the $y = 0.5H$ plane.

Table 4

Nusselt number values for the natural convection of pure fluids in a hotstrip.

Ra	d=0.4H		d=0.5H							
	Air	Water	Air		Water					
	Vert. w.	Top	Left w.	Top	Right w.	Left w.	Top	Right w.		
10^3	1.500	0.781	1.500	0.781	1.281	0.806	1.898	1.279	0.805	1.898
10^4	1.827	0.579	1.827	0.587	1.817	0.657	2.068	1.815	0.659	2.064
10^5	3.885	0.561	3.924	0.694	3.828	0.600	3.769	3.863	0.707	3.766

When hotstrip is placed in the centre ($d=0.4H$) we present values for heat flux from vertical walls and the top wall. When the hotstrip is placed off-centre ($d=0.5H$) the symmetry is broken and results for vertical walls are given separately.

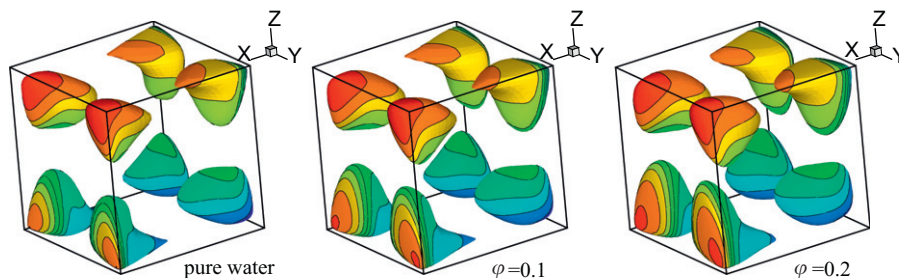


Fig. 7. Isosurfaces of $|v_y| = 5$ for water and Cu nanofluid for natural convection in a differentially heated cubic cavity; $Ra = 10^6$. Contours of temperature $-0.4(0.1)0.4$ are displayed on the isosurfaces.

Table 5
Nusselt number values for natural convection of nanofluids in a hotstrip.

Ra	φ	Water+Cu		Water+Al ₂ O ₃		Water+TiO ₂	
		Vert. w.	Top	Vert. w.	Top	Vert. w.	Top
10 ³	0.1	1.984	1.062	1.961	1.052	1.888	1.012
10 ³	0.2	2.591	1.409	2.535	1.381	2.357	1.283
10 ⁴	0.1	2.185	0.862	2.146	0.861	2.075	0.824
10 ⁴	0.2	2.711	1.245	2.637	1.237	2.460	1.140
10 ⁵	0.1	4.318	0.798	4.183	0.791	4.080	0.766
10 ⁵	0.2	4.540	0.965	4.242	0.951	4.048	0.887

The hotstrip is located in the central position, $d=0.4H$.

Table 6
Nusselt number values for natural convection of nanofluids in a hotstrip.

Ra	φ	Water+Cu			Water+Al ₂ O ₃			Water+TiO ₂		
		Left v.	Top	Right v.	Left v.	Top	Right v.	Left v.	Top	Right v.
10 ³	0.1	1.682	1.094	2.520	1.662	1.083	2.492	1.601	1.042	2.399
10 ³	0.2	2.192	1.450	3.299	2.143	1.422	3.228	1.993	1.320	3.000
10 ⁴	0.1	2.029	0.916	2.626	1.980	0.912	2.589	1.923	0.874	2.497
10 ⁴	0.2	2.393	1.294	3.364	2.311	1.283	3.283	2.164	1.183	3.056
10 ⁵	0.1	4.339	0.908	4.008	4.216	0.905	3.880	4.105	0.872	3.785
10 ⁵	0.2	4.680	1.186	4.341	4.390	1.163	4.120	4.182	1.084	3.896

The hotstrip is located in the off-central position, $d=0.5H$.

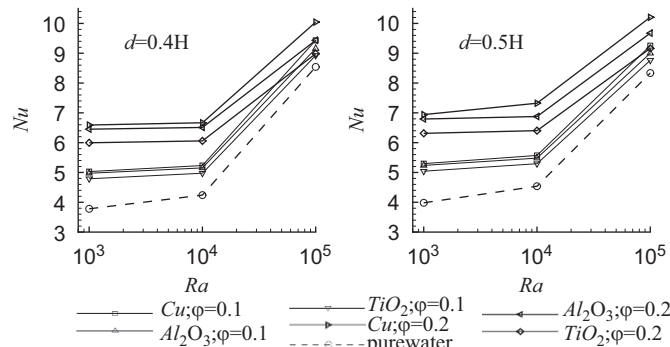


Fig. 8. Total heat flux transferred from the hotstrip into the fluid presented with Nusselt number. Hotstrip is located in the centre of the cavity (left) and off-centre (right).

flux in terms of Nusselt versus Rayleigh number value. We observe that the greatest improvement in heat transfer can be achieved in the case of low Rayleigh number. At low Ra conduction plays an important role in heat transfer and since nanofluids have a substantially increased thermal conductivity compared to pure fluid, conduction is more effective. As the Rayleigh number value is increased, the most of the heat transfer occurs due to convection and thermal conductivity plays a less important role—thus usage of nanofluids brings relatively lower heat transfer enhancement. Comparing the three nanofluids used in simulations we observe that in all cases Cu nanofluid yields the highest heat fluxes, Al₂O₃ the second highest and TiO₂ the lowest. However, all are well above the heat flux obtained by pure water. Similar findings were reported by Oztop and Abu-Nada [20] for a two-dimensional natural convection simulation. Simulations were performed with two solid particle volume fractions for nanofluids: $\varphi = 0.1$ and 0.2 . In all cases we observe that increasing the solid particle volume fraction increases the heat transfer. In

the conduction dominated flows we observe that the heat transfer enhancement observed when comparing pure water and $\varphi = 0.1$ nanofluid is about the same as when comparing $\varphi = 0.1$ and 0.2 nanofluids. Thus, heat transfer enhancement for conduction dominated flows is an approximately linear function of solid volume fraction. This can be explained by examining the Maxwell–Garnet formula (8) for thermal conductivity of nanofluids in the limit of low particle volume fractions:

$$\lim_{\varphi \rightarrow 0} k_{nf} = k_f \left(1 - 3 \frac{k_f - k_s}{k_s + 2k_f} \varphi \right), \quad (19)$$

where second order φ^2 terms were omitted. Thus, for low solid particles volume fractions thermal conductivity of nanofluids behaves approximately as a linear function of solid volume fraction.

Temperature contours on the central $y=0.5H$ plane for natural convection of Cu nanofluid in a hotstrip are shown in Fig. 9. As in the natural convection in a differentially heated cavity case, the temperature distribution for other nanofluids is very similar to the temperature distribution of Cu nanofluid. Comparison between pure water and Cu nanofluid is made for both locations of the hotstrip. In the low Ra conduction dominated case the largest differences between temperature contours of pure fluid and nanofluids can be observed away from the hot and cold walls. This makes the temperature gradient on the walls equal in all cases and the increase in heat flux can be attributed to the increased thermal conductivity of nanofluids. As we increase the Rayleigh number, the differences in temperature fields become larger throughout the whole flow fields. Examining the temperature field close to the hotstrip we observe that pure fluid temperature contours are closest to the wall, although the differences are not large. This has been observed in the case of natural convection in a differentially heated cavity also. The consequence of this is that the wall temperature gradients are highest in the pure fluid case.

With the increase of Ra number the temperature contours move away from the top wall of the hotstrip, making temperature gradient and hence the heat transfer from the top wall smaller. This phenomenon occurs for pure fluids and for nanofluids. Since only a small part of the total heat transfer occurs from the top wall, the total heat transfer still increases with increasing Rayleigh number. Increased Ra produces larger buoyancy forces and higher fluid velocities. In the high Ra case there is a large quantity of hot fluid rising upward above the top of the hotstrip making the temperature gradient on top of the hotstrip smaller. This effect is stronger in the case when hotstrip is located in the centre, since the broken symmetry of the off-central position makes the fluid rise not exactly on top of the hotstrip and thus enabling higher temperature gradients.

Due to inherent physical instability of fluid being heated from below, steady solution of this problem may not be sufficient. If the Rayleigh number would be higher, the problem should be simulated as time dependent.

We examine heat flux distribution in terms of the local Nusselt number on a profile across the centre of the hotstrip in Fig. 10. The largest heat flux values are found near the edges connecting the vertical and top walls. There the convection dominates and ensures the highest heat flux. The smallest heat flux is located on the top wall, where fluid flow is very slow and conduction dominates the heat transfer in all cases. In the $Ra=10^3$ case, clear heat transfer enhancement can be observed when comparing pure water with nanofluids. At $Ra=10^5$ in the case of convection dominated vertical walls this enhancement is smaller, while substantial enhancement can be observed on the top wall, where conduction still governs the heat transfer.

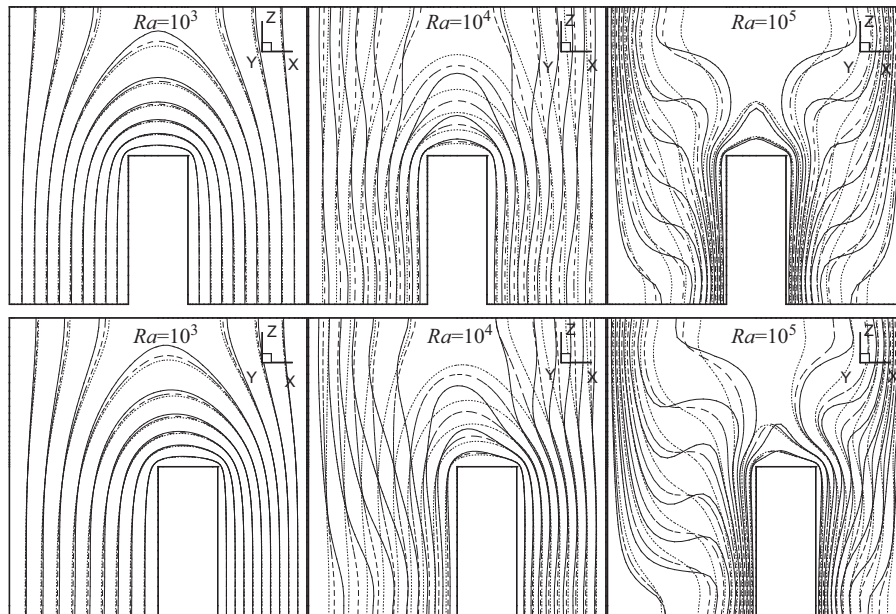


Fig. 9. Temperature contours on the central $y = 0.5H$ plane for natural convection in a hotstrip located in the centre (top) and off-centre (bottom). Contour values are $-0.4(0.1)0.4$. Solid line denotes pure water, dashed line $\varphi = 0.1$ Cu nanofluid and dotted line $\varphi = 0.2$ Cu nanofluid.

Three-dimensional structure of the flow field is shown in Fig. 11. We present isosurfaces of the $|v_y| = 2.5$ component of the velocity field for pure water and Cu nanofluid. The y component is directed normal to the main vortical motion, i.e. it is the direction that a two-dimensional case would consider to be irrelevant. We observe that the v_y is indeed small compared to the velocities in other two directions in the low Ra case. But when the Rayleigh number is increased, the flow in the y direction is not to be neglected. The maximal velocity v_y amounts to about 10% of the horizontal velocity v_x . Furthermore, we observe that using nanofluids the flow fields become more three-dimensional as compared to pure water. Using nanofluids does not significantly change the maximal value of v_y but it does, as it is evident from Fig. 11, substantially enlarge the area where v_y velocity components are significant. Off-central position of the hotstrip results in a more pronounced three-dimensional flow field than the central position of the hotstrip. The loss of symmetry contributes to the three-dimensional structure of the flow.

5.4. Relationship between vorticity, vorticity flux and heat transfer intensity

Relationship between heat transfer intensity and vorticity has been studied for pure fluids by Chang et al. [5]. Our numerical method employs vorticity as one of the unknown flow fields. Moreover usage of the boundary element method enables computation of normal derivatives of vorticity on the boundaries. Thus vorticity and vorticity flux on the boundary are a part of the solution of our numerical algorithm. No additional post-processing of the results is necessary, thus avoiding additional numerical errors in the solution.

We will examine vorticity flux on vertical walls in the (y,z) plane. We define the vorticity wall integral I_{ω_y} and vorticity flux wall integral I_{q_y} as

$$I_{\omega_y} = \int_{\Gamma} \omega_y d\Gamma, \quad I_{q_y} = \int_{\Gamma} \vec{\nabla} \omega_y \cdot \vec{n} d\Gamma. \quad (20)$$

Fig. 12 shows the dependence of heat transfer, vorticity and

vorticity flux integrals for Cu nanofluid with 0.2 particle volume fraction. We observe that all quantities increase with increasing Rayleigh number. The rate of increase is approximately exponential. This makes values of vorticity and vorticity flux on the wall a good indicator of heat transfer intensity. The physical reason for this fact is that for a wall in the (y,z) plane ω_y vorticity component measures the wall normal gradient of velocity, i.e. $\omega_y|_{wall} = \partial v_z / \partial x$. Since with increasing Ra the velocity boundary layer becomes thinner and velocity gradients increase, the vorticity is thus increased as well. In the cases we considered, convection was the dominant heat transfer mechanism. In convection dominated flows there is a relationship between thermal and velocity boundary layers and therefore a relationship between vorticity and heat transfer. The vorticity flux, i.e. the normal derivative of vorticity, is a measure for the rate of change of velocity gradient in the normal direction away from the wall. It too increases with Ra in approximately the same way as the Nusselt number.

6. Summary

The paper presents a numerical method for the simulation of flow of nanofluids. The method is based on the combination of single domain and subdomain BEM used to solve the velocity–vorticity formulation of Navier–Stokes equations. We developed a dynamic solver accuracy algorithm, which was used to speed up the simulations. CPU times were decreased by up to 50%.

The developed algorithm was used to simulate flow of three types of water based nanofluids in two test cases: natural convection in a three-dimensional differentially heated cavity and natural convection around a hotstrip. The main findings are: (i) using water based nanofluids instead of pure water enhances heat transfer, (ii) the enhancement is largest when conduction is the dominant heat transfer mechanism, since in this case the increased heat conductivity of the nanofluid makes all the difference, (iii) in convection dominated flows heat transfer enhancement is smaller, (iv) all considered nanofluids (Cu, Al_2O_3 and TiO_2) enhanced heat transfer for approximately the same

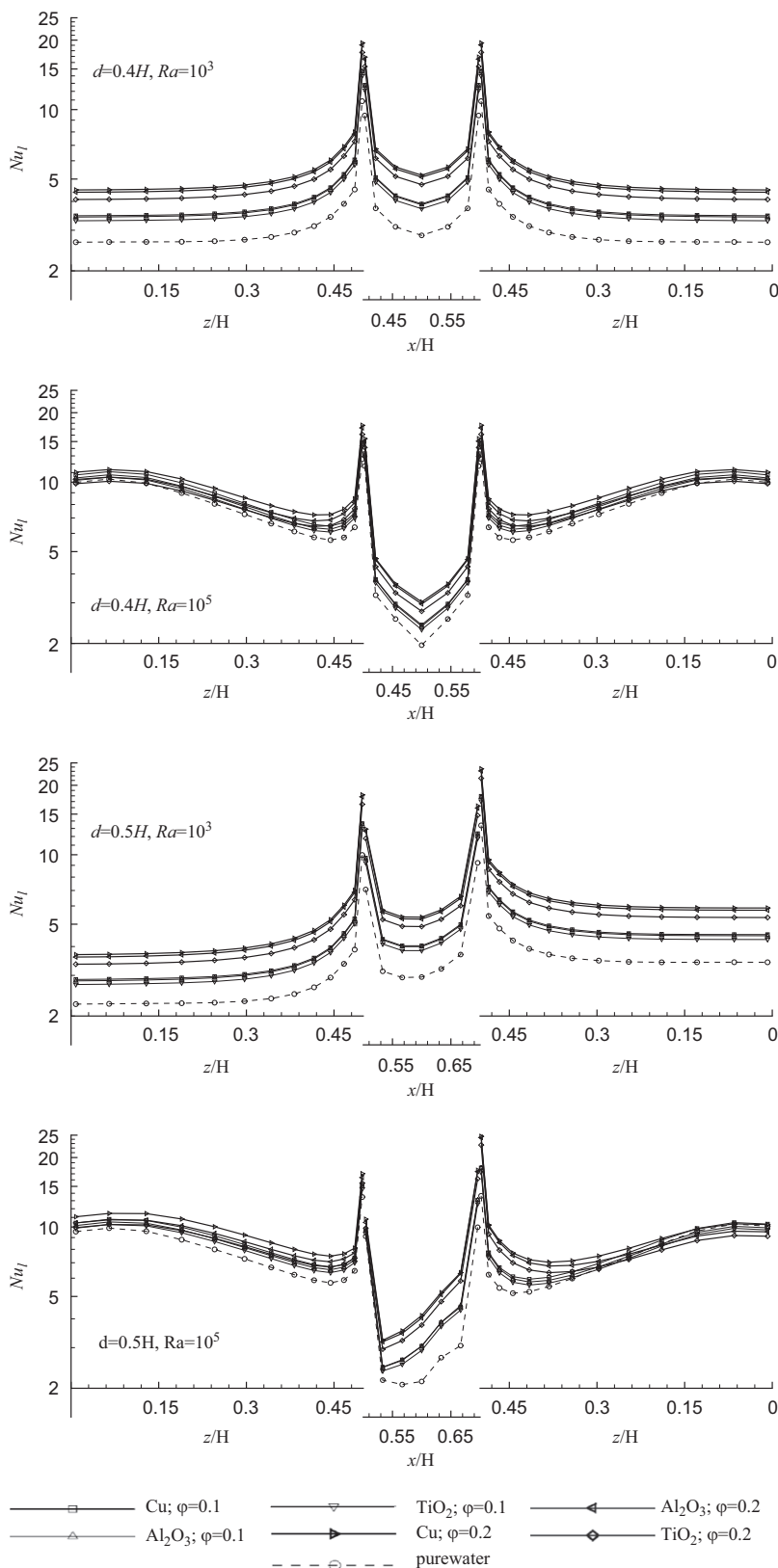


Fig. 10. Heat flux shown in terms of local Nusselt number on a profile across the hotstrip on the $y = 0.5H$ plane. The left profile starts at $(d,0.5H,0)$ going up the left vertical wall, across the top wall and down the right vertical wall.

order of magnitude, Cu nanofluid giving the best results, (v) heat transfer enhancement grows with increasing solid particle volume fraction in the nanofluid, (vi) the differences between temperature fields when using different nanofluids with the same

solid nanoparticle volume fraction are small, (vii) vorticity and vorticity flux may be used as an indicator for heat transfer intensity of nanofluids, since they grow with Rayleigh number in approximately the same way as the Nusselt number value, (viii)

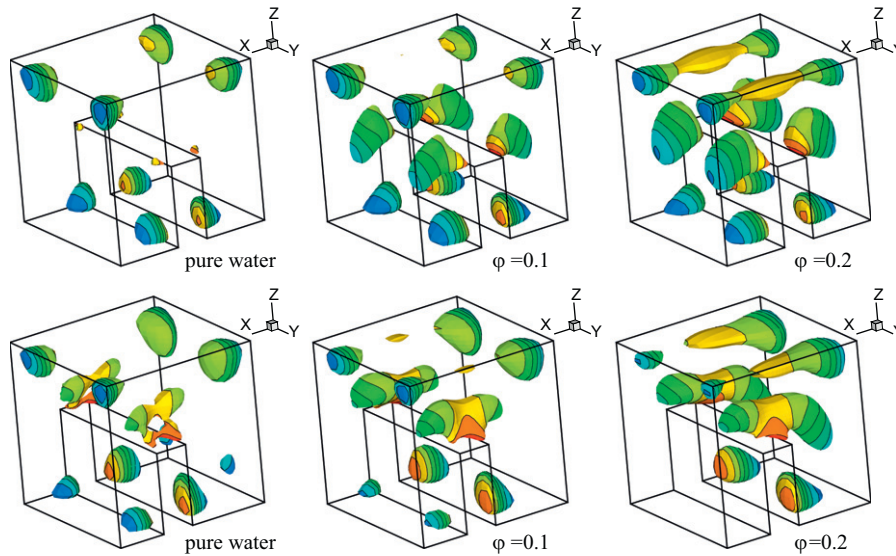


Fig. 11. Isosurfaces of $|v_y|=2.5$ for water and Cu nanofluid for natural convection in a hotstrip; $Ra = 10^5$. Contours of temperature $-0.4(0.1)0.4$ are displayed on the isosurfaces. Top row $d=0.4H$, bottom row $d=0.5H$.

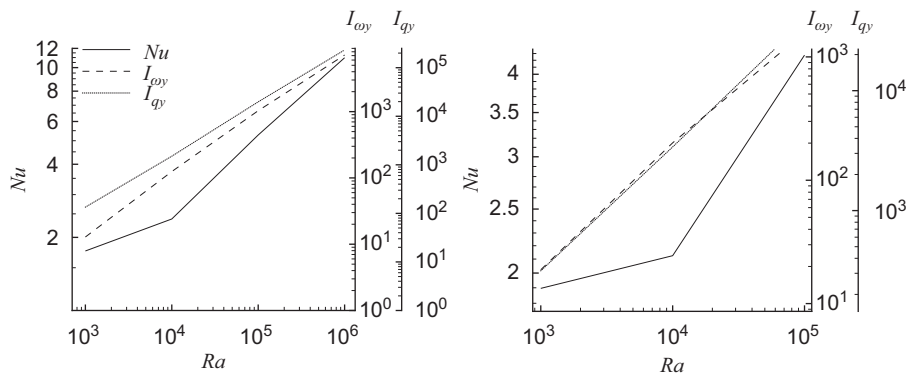


Fig. 12. Relationship between heat transfer (Nu), vorticity integral I_{ω_y} and vorticity flux integral I_{q_y} for natural convection in a differentially heated cavity (left) and in a hotstrip ($d=0.4H$) (right) using Cu nanofluid with nanoparticle solid volume fraction 0.2.

examining the three-dimensional structure of the flow fields, we discovered that the flow is more three-dimensional when using nanofluids.

References

- [1] Abu-Nada E. Application of nanofluids for heat transfer enhancement of separated flows encountered in a backward facing step. *Int J Heat Fluid Flow* 2008;29:242–9.
- [2] Abu-Nada E, Oztop HF. Effects of inclination angle on natural convection in enclosures filled with cuwater nanofluid. *Int J Heat Fluid Flow* 2009;30:669–78.
- [3] Akbarinia A, Behzadmehr A. Numerical study of laminar mixed convection of a nanofluid in horizontal curved tubes. *Appl Thermal Eng* 2007;27:1327–37.
- [4] Brinkman HC. The viscosity of concentrated suspensions and solutions. *J Chem Phys* 1952;20:571–81.
- [5] Chang L-M, Wang L-B, Song K-W, Sun D-L, Fan J-F. Numerical study of the relationship between heat transfer enhancement and absolute vorticity flux along main flow direction in a channel formed by a flat tube bank fin with vortex generators. *Int J Heat Mass Transfer* 2009;52:1794–801.
- [6] Choi SUS. Enhancing thermal conductivity of fluids with nanoparticles. *Dev Appl Non Newtonian Flows* 1995;66:99–106.
- [7] Corvaro F, Paroncini M. A numerical and experimental analysis on the natural convective heat transfer of a small heating strip located on the floor of a square cavity. *Appl Thermal Eng* 2008;28:25–35.
- [8] Corvaro F, Paroncini M. An experimental study of natural convection in a differentially heated cavity through a 2D-PIV system. *Int J Heat Mass Transfer* 2009;52:355–65.
- [9] Daube O. Resolution of the 2D Navier–Stokes equations in velocity–vorticity form by means of an influence matrix technique. *J Comput Phys* 1992;103:402–14.
- [10] Einstein A. Investigation on the theory of Brownian motion. New York: Dover; 1956.
- [11] Gümgüm S, Tezer-Sezgin M. DRBEM solution of natural convection flow of nanofluids with a heat source. *Eng Anal Bound Elem* 2010;34(8):727–37.
- [12] Ho CJ, Chen MW, Li ZW. Numerical simulation of natural convection of nanofluid in a square enclosure: effects due to uncertainties of viscosity and thermal conductivity. *Int J Heat Mass Transfer* 2008;51:4506–16.
- [13] Hwang KS, Lee J-H, Jang SP. Buoyancy-driven heat transfer of water-based Al_2O_3 nanofluids in a rectangular cavity. *Int J Heat Mass Transfer* 2007;50:4003–10.
- [14] Khanafer K, Vafai K, Lightstone M. Buoyancy-driven heat transfer enhancement in a two-dimensional enclosure utilizing nanofluids. *Int J Heat Mass Transfer* 2003;46:3639–53.
- [15] Liu CH. Numerical solution of three-dimensional Navier Stokes equations by a velocity–vorticity method. *Int J Numer Meth Fluids* 2001;35:533–57.
- [16] Lo DC, Young DL, Murugesan K, Tsai CC, Gou MH. Velocity–vorticity formulation for 3D natural convection in an inclined cavity by DQ method. *Int J Heat Mass Transfer* 2007;50:479–91.
- [17] Maxwell JC. A treatise on electricity and magnetism. 2nd ed.. Oxford, UK: Clarendon Press; 1881.
- [18] Mirmasoumi S, Behzadmehr A. Effect of nanoparticles mean diameter on mixed convection heat transfer of a nanofluid in a horizontal tube. *Int J Heat Fluid Flow* 2008;29:557–66.

- [19] Ögüt EB. Natural convection of water-based nanofluids in an inclined enclosure with a heat source. *International Journal of Thermal Sciences* 2009;48:2063–73.
- [20] Oztop HF, Abu-Nada E. Natural convection of water-based nanofluids in an inclined enclosure with a heat source. *Int J Heat Fluid Flow* 2008;29:1326–36.
- [21] Paige CC, Saunders MA. LSQR: an algorithm for sparse linear equations and sparse least squares. *ACM Trans Math Software* 1982;8:43–71.
- [22] Popov V, Power H, Škerget L. Domain decomposition techniques for boundary elements: applications to fluid flow. WIT press; 2007.
- [23] Ramšak M, Škerget L, Hriberšek M, Žunič Z. A multidomain boundary element method for unsteady laminar flow using stream function vorticity equations. *Eng Anal Bound Elem* 2005;29:1–14.
- [24] Ravnik J, Škerget L. Natural convection around a 3D hotstrip simulated by BEM. In: *Mesh reduction methods BEM/MRM*, vol. XXXI, 2009, p. 343–52.
- [25] Ravnik J, Škerget L, Žunič Z. Velocity–vorticity formulation for 3D natural convection in an inclined enclosure by BEM. *Int J Heat Mass Transfer* 2008;51:4517–27.
- [26] Ravnik J, Škerget L, Žunič Z. Combined single domain and subdomain BEM for 3D laminar viscous flow. *Eng Anal Bound Elem* 2009;33:420–4.
- [27] Ravnik J, Škerget L, Žunič Z. Fast single domain–subdomain BEM algorithm for 3D incompressible fluid flow and heat transfer. *Int J Numer Meth Eng* 2009;77:1627–45.
- [28] Shukla RK, Dhir VK. Numerical study of the effective thermal conductivity of nanofluids. In: *ASME summer heat transfer conference*, 2005.
- [29] Škerget L, Hriberšek M, Žunič Z. Natural convection flows in complex cavities by BEM. *Int J Num Meth Heat Fluid Flow* 2003;13:720–35.
- [30] Tiwari RK, Das MK. Heat transfer augmentation in a two-sided lid-driven differentially heated square cavity utilizing nanofluids. *Int J Heat Mass Transfer* 2007;50:2002–18.
- [31] Torii S. Turbulent heat transfer behavior of nanofluid in a circular tube heated under constant heat flux. *Advances in Mechanical Engineering*, 2010: 2010; 7 (Article ID 917612).
- [32] Tric E, Labrosse G, Betrouni M. A first incursion into the 3D structure of natural convection of air in a differentially heated cubic cavity, from accurate numerical simulations. *Int J Heat Mass Transfer* 2000;43:4034–56.
- [33] Wang X-Q, Mujumdar AS. Heat transfer characteristics of nanofluids: a review. *Int J Thermal Sci* 2007;46:1–19.
- [34] Wong KL, Baker AJ. A 3D incompressible Navier–Stokes velocity–vorticity weak form finite element algorithm. *Int J Num Meth Fluids* 2002;38:99–123.
- [35] Yang Y, Zhang ZG, Grulke EA, Anderson WB, Wu G. Heat transfer properties of nanoparticle-in-fluid dispersions (nanofluids) in laminar flow. *Int J Heat Mass Transfer* 2005;48:1107–16.